

Iron(II) Complexes of 2,6-Di(*1H*-pyrazol-3-yl)pyridine Derivatives with Hydrogen Bonding and Sterically Bulky Substituents

Thomas D. Roberts^a, Marc A. Little^{a,b}, Laurence J. Kershaw Cook^a
and Malcolm A. Halcrow*^a

^a*School of Chemistry, University of Leeds, Woodhouse Lane, Leeds, UK LS2 9JT.*

E-mail: m.a.halcrow@leeds.ac.uk

^b*Current address: Department of Chemistry, University of Liverpool, Crown Street,
Liverpool, UK L69 7ZD.*

Supporting Information

Figure S1. View of the asymmetric unit of $\mathbf{1}[\text{ClO}_4]_2 \cdot 2(\text{C}_2\text{H}_5)_2\text{O} \cdot \text{CH}_3\text{NO}_2$, showing the full atom numbering scheme.

Figure S2. View of the asymmetric unit of $\mathbf{2}[\text{BF}_4]_2 \cdot 3\text{CH}_3\text{CN}$, showing the full atom numbering scheme.

Table S1 Selected bond lengths and angles in the crystal structure of $\mathbf{1}[\text{ClO}_4]_2 \cdot 2(\text{C}_2\text{H}_5)_2\text{O} \cdot \text{CH}_3\text{NO}_2$.

Table S2 Selected bond lengths and angles in the crystal structures of $\mathbf{2}[\text{BF}_4]_2 \cdot 3\text{CH}_3\text{CN}$ and $\mathbf{2}[\text{ClO}_4]_2 \cdot 3\text{CH}_3\text{CN}$.

Figure S3. Packing diagram of $\mathbf{2}[\text{BF}_4]_2 \cdot 3\text{CH}_3\text{CN}$, showing its association into 1D ladder chains through N–H...F hydrogen bonding.

Figure S4. View of the two unique complex dication in the crystal structure of $\mathbf{3}[\text{BF}_4]_2 \cdot x\text{CF}_3\text{CH}_2\text{OH} \cdot y(\text{C}_3\text{H}_7)_2\text{O}$, showing the atom numbering scheme.

Figure S5. View of molecules A and B in $\mathbf{3}[\text{BF}_4]_2 \cdot x\text{CF}_3\text{CH}_2\text{OH} \cdot y(\text{C}_3\text{H}_7)_2\text{O}$, emphasising the S-shaped ligand conformations and showing intermolecular contacts that probably give rise to them.

Figure S6. View of the asymmetric unit of $\mathbf{3}[\text{BF}_4]_2 \cdot x\text{CF}_3\text{CH}_2\text{OH} \cdot y(\text{C}_3\text{H}_7)_2\text{O}$, showing the hydrogen bonds in the crystal lattice.

Table S3 Selected bond lengths and angles in the crystal structure of $\mathbf{3}[\text{BF}_4]_2 \cdot x\text{CF}_3\text{CH}_2\text{OH} \cdot y(\text{C}_3\text{H}_7)_2\text{O}$.

Figure S7. Comparison of the helical, interpenetrating hydrogen bond topology in $\mathbf{3}[\text{BF}_4]_2 \cdot x\text{CF}_3\text{CH}_2\text{OH} \cdot y(\text{C}_3\text{H}_7)_2\text{O}$ with a (10,3)-a net.

Figure S8. View of the $[\text{Fe}(\text{L}^4)_2][\text{BF}_4]_2 \cdot 2(\text{C}_2\text{H}_5)_2\text{O} \cdot \text{CF}_3\text{CH}_2\text{OH}$ assembly in $\mathbf{4}[\text{BF}_4]_2 \cdot x\text{CF}_3\text{CH}_2\text{OH} \cdot y(\text{C}_2\text{H}_5)_2\text{O}$, showing the full atom numbering scheme.

Table S4 Selected bond lengths and angles in the crystal structure of $\mathbf{4}[\text{BF}_4]_2 \cdot x\text{CF}_3\text{CH}_2\text{OH} \cdot y(\text{C}_2\text{H}_5)_2\text{O}$.

Table S5 Hydrogen bond parameters for the crystal structures in this work.

Table S6 Connections making up the hydrogen-bonded networks in this study.

Definitions of the structural parameters discussed in the main paper.

Scheme S1. Angles used in the definitions of the coordination distortion parameters Σ and Θ .

Scheme S2. Definition of the Jahn-Teller distortion parameters θ and ϕ .

Figure S9. Variable temperature magnetic susceptibility behaviour of $\mathbf{2}[\text{BF}_4]_2 \cdot \text{H}_2\text{O}$, $\mathbf{2}[\text{ClO}_4]_2 \cdot 2\text{H}_2\text{O}$, $\mathbf{3}[\text{BF}_4]_2 \cdot \text{H}_2\text{O}$ and $\mathbf{4}[\text{BF}_4]_2 \cdot \frac{1}{2}\text{CF}_3\text{CH}_2\text{OH}$ (red diamonds).

Figure S10. Variable temperature magnetic susceptibility behaviour of $\mathbf{1}[\text{ClO}_4]_2 \cdot 2\text{H}_2\text{O}$.

References

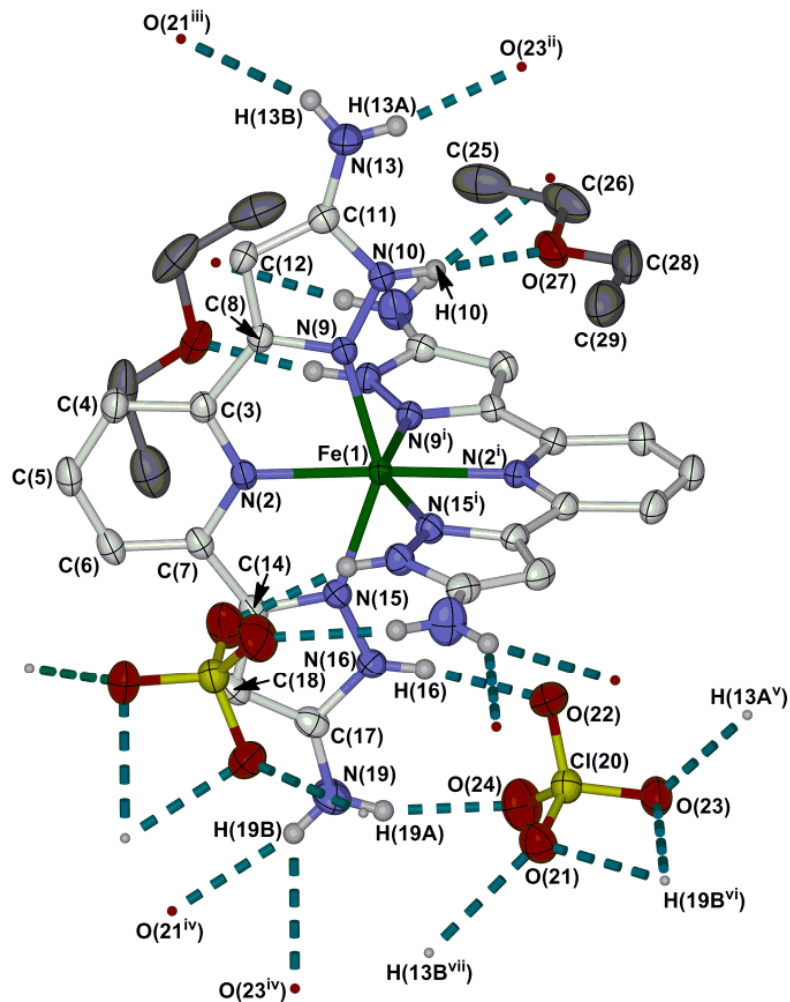


Fig. S1. View of the asymmetric unit of $\mathbf{1}[\text{ClO}_4]_2 \cdot 2(\text{C}_2\text{H}_5)_2\text{O} \cdot \text{CH}_3\text{NO}_2$, showing the full atom numbering scheme. Atomic displacement ellipsoids are at the 50 % probability level. The disordered nitromethane solvent molecule does not take part in hydrogen bonding interactions, and is not shown. C-bound H atoms have been omitted for clarity. Symmetry codes: (i) $1-x, y, \frac{1}{2}-z$; (ii) $\frac{1}{2}+x, \frac{3}{2}-y, -z$; (iii) $\frac{1}{2}+x, \frac{1}{2}+y, \frac{1}{2}-z$; (iv) $x, 1-y, \frac{1}{2}+z$; (v) $-\frac{1}{2}+x, \frac{3}{2}-y, -z$; (vi) $x, 1-y, -\frac{1}{2}+z$; (vii) $-\frac{1}{2}+x, -\frac{1}{2}+y, \frac{1}{2}-z$.

Colour code: C {complex}, white; C {solvent}, dark grey; H, grey; Cl, yellow; Fe, green; N, pale blue; O, red.

The view is the same as Fig. 1 of the main paper.

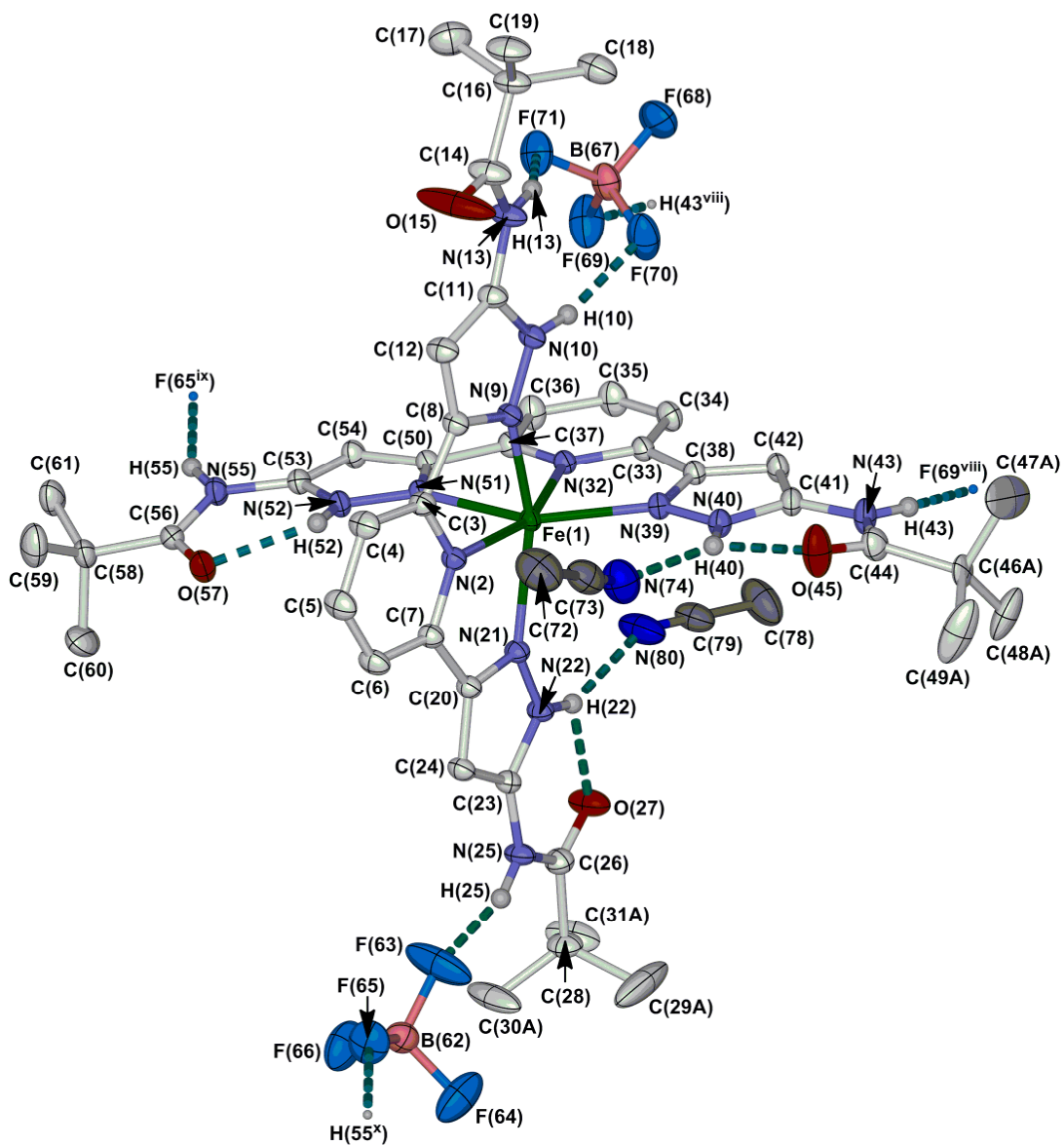


Fig. S2. View of the asymmetric unit of $\mathbf{2}[\text{BF}_4]_2 \cdot 3\text{CH}_3\text{CN}$, showing the full atom numbering scheme. Atomic displacement ellipsoids are at the 50 % probability level. Only one orientation of the disordered *tert*butyl groups is included and solvent molecule C(75)-N(77), which does not take part in hydrogen bonding interactions, is not shown. C-bound H atoms have been omitted for clarity. Symmetry codes: (viii) $-x, -y, -z$; (ix) $-1+x, y, z$; (x) $1+x, y, z$.

Colour code: C {complex}, white; C {solvent}, dark grey; H, grey; B, pink; F, cyan; Fe, green; N {complex}, pale blue; N {solvent}, dark blue; O, red.

The salt $[\text{Fe}(\text{L}^2)_2][\text{ClO}_4]_2 \cdot 3\text{CH}_3\text{CN}$ is isostructural with this one and has an identical atom numbering scheme, but with atoms B(62)-F(71) replaced by Cl(62)-O(71) as appropriate.

Table S1 Selected bond lengths and angles in the crystal structure of **1**[ClO₄]₂·2(C₂H₅)₂O·CH₃NO₂ (Å, °).^a See Fig. S1 for the atom numbering scheme.

Fe(1)–N(2)	2.1567(12)
Fe(1)–N(9)	2.1888(13)
Fe(1)–N(15)	2.1936(12)
N(2)–Fe(1)–N(2 ⁱ) (ϕ)	177.33(6)
N(2)–Fe(1)–N(9)	73.67(5)
N(2)–Fe(1)–N(9 ⁱ)	108.22(4)
N(2)–Fe(1)–N(15)	73.19(5)
N(2)–Fe(1)–N(15 ⁱ)	104.90(5)
N(9)–Fe(1)–N(9 ⁱ)	94.92(7)
N(9)–Fe(1)–N(15)	146.87(5)
N(9)–Fe(1)–N(15 ⁱ)	95.15(5)
N(15)–Fe(1)–N(15 ⁱ)	93.42(7)
θ	87.91(1)

^a Symmetry code: (i) 1– x , y , $1/2-z$.

Table S2 Selected bond lengths and angles in the crystal structures of **2**[BF₄]₂·3CH₃CN and **2**[ClO₄]₂·3CH₃CN (Å, °). See Fig. S2 for the atom numbering scheme.

	X [−] = BF ₄ [−]	X [−] = ClO ₄ [−]
Fe(1)–N(2)	2.1333(11)	2.134(2)
Fe(1)–N(9)	2.1864(11)	2.1952(15)
Fe(1)–N(21)	2.2214(11)	2.2291(18)
Fe(1)–N(32)	2.1562(11)	2.163(2)
Fe(1)–N(39)	2.1654(11)	2.174(2)
Fe(1)–N(51)	2.2138(11)	2.2268(19)
N(2)–Fe(1)–N(9)	73.99(4)	74.24(7)
N(2)–Fe(1)–N(21)	74.47(4)	74.41(7)
N(2)–Fe(1)–N(32) (ϕ)	158.30(4)	158.91(7)
N(2)–Fe(1)–N(39)	125.84(4)	125.39(7)
N(2)–Fe(1)–N(51)	86.73(4)	87.07(8)
N(9)–Fe(1)–N(21)	148.03(4)	148.23(8)
N(9)–Fe(1)–N(32)	99.88(4)	99.78(7)
N(9)–Fe(1)–N(39)	92.19(4)	91.88(7)
N(9)–Fe(1)–N(51)	90.13(4)	90.10(6)
N(21)–Fe(1)–N(32)	111.41(4)	111.39(6)
N(21)–Fe(1)–N(39)	102.06(4)	102.07(7)
N(21)–Fe(1)–N(51)	93.16(4)	93.34(7)
N(32)–Fe(1)–N(39)	74.46(4)	74.31(7)
N(32)–Fe(1)–N(51)	72.32(4)	72.57(8)
N(39)–Fe(1)–N(51)	146.60(4)	146.67(8)
θ	89.67(1)	89.01(2)

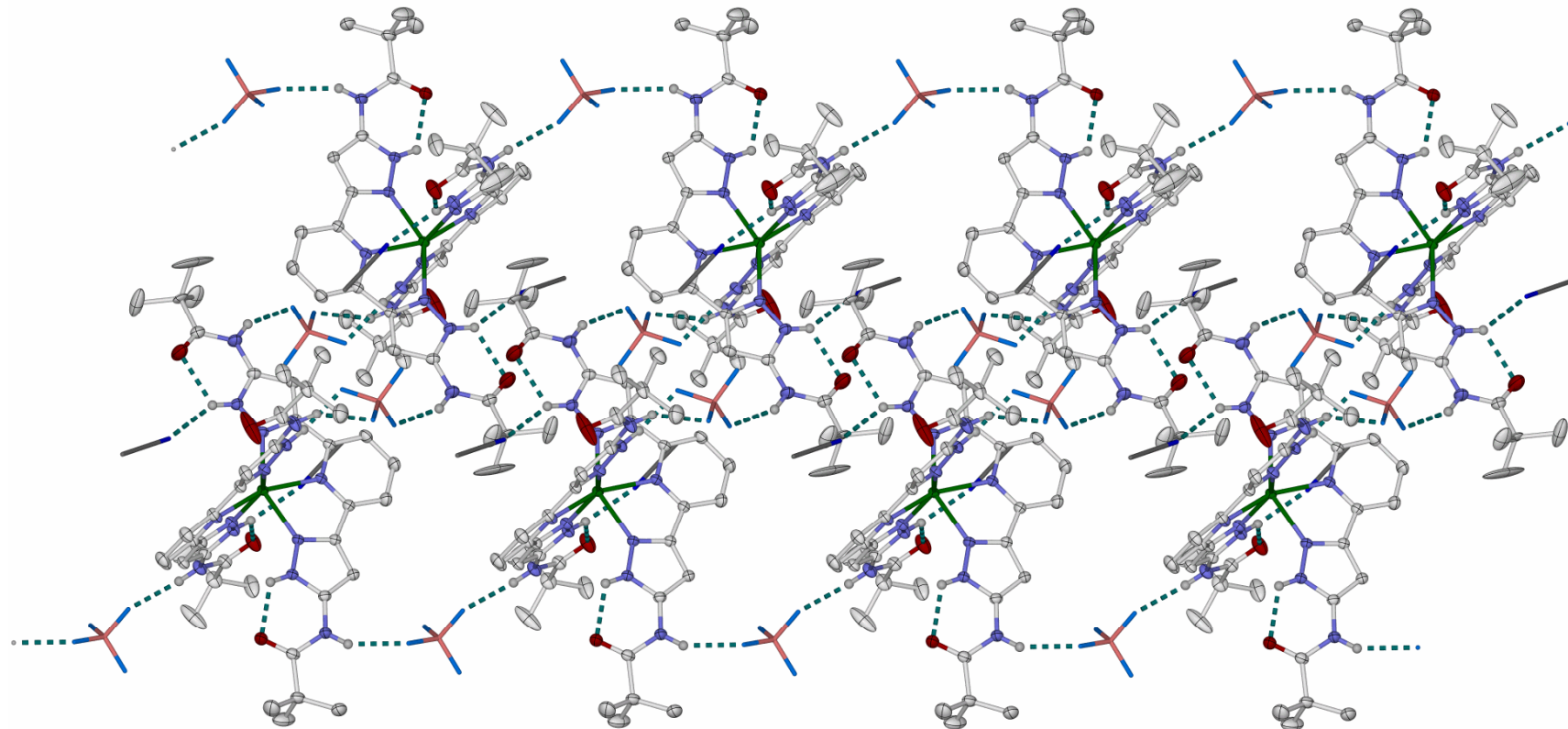


Fig. S3. Packing diagram of $2[\text{BF}_4]_2 \cdot 3\text{CH}_3\text{CN}$, showing its association into 1D ladder chains through N–H...F hydrogen bonding. Atomic displacement ellipsoids are at the 50 % probability level for the complex molecules, while other atoms have arbitrary radii. The view is perpendicular to the [021] vector, with the *a* axis horizontal. Only one orientation of the disordered *tert*butyl groups is shown, and the solvent molecule that does not take part in hydrogen bonding has been omitted for clarity.

Colour code: C {complex}, white; C {solvent}, dark grey; H, grey; B, pink; F, cyan; Fe, green; N {complex}, pale blue; N {solvent}, dark blue; O, red.

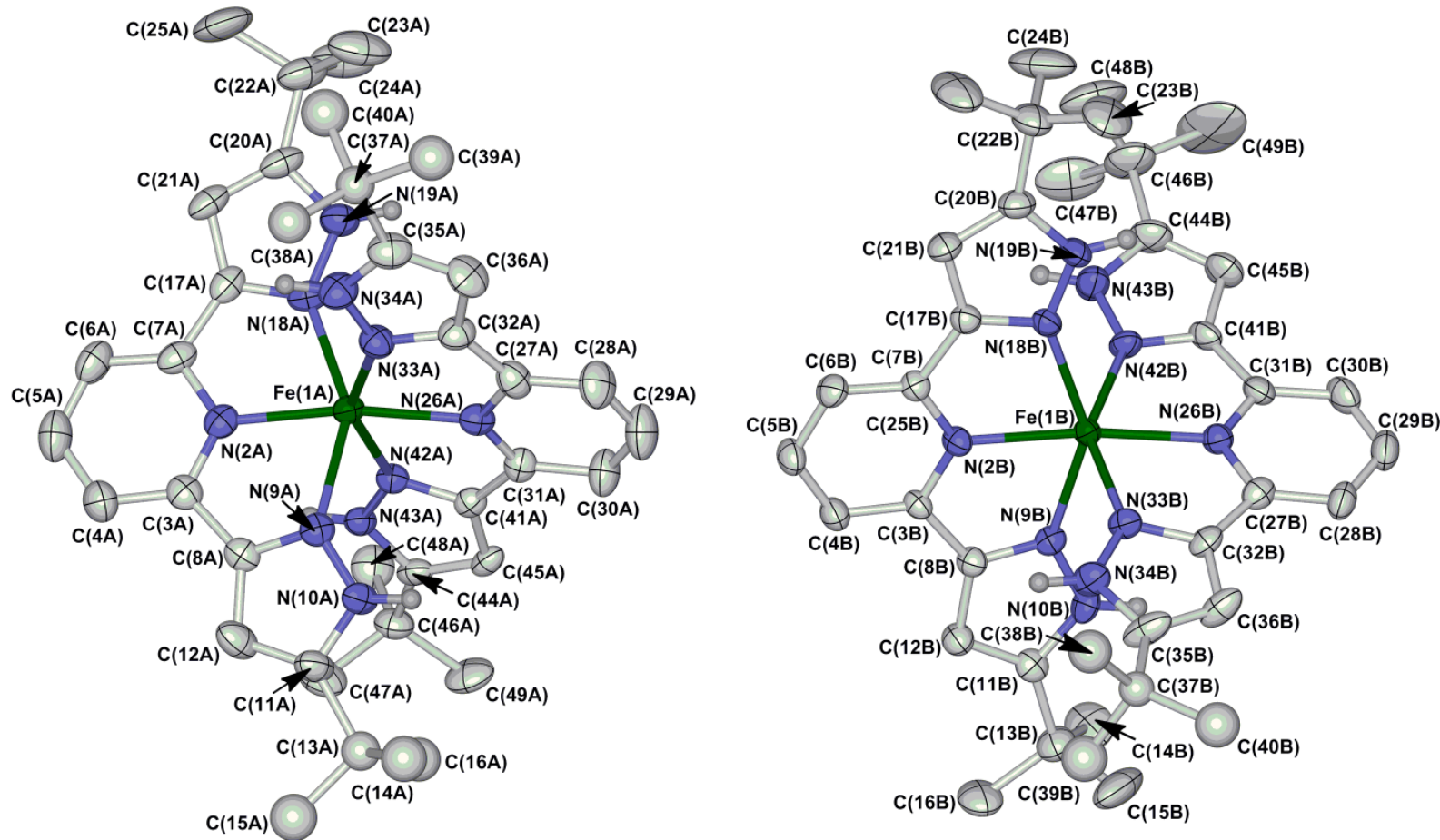


Fig. S4. View of the two unique complex dications in the crystal structure of $\mathbf{3}[\text{BF}_4]_2 \cdot x\text{CF}_3\text{CH}_2\text{OH} \cdot y(\text{C}_3\text{H}_7)_2\text{O}$, showing the atom numbering scheme employed. Atomic displacement ellipsoids are at the 50 % probability level. Only one orientation is included of the three disordered *tert*butyl groups in the model, and C-bound H atoms have been omitted for clarity.

Colour code: C, white; H, pale grey; Fe, green; N, pale blue.

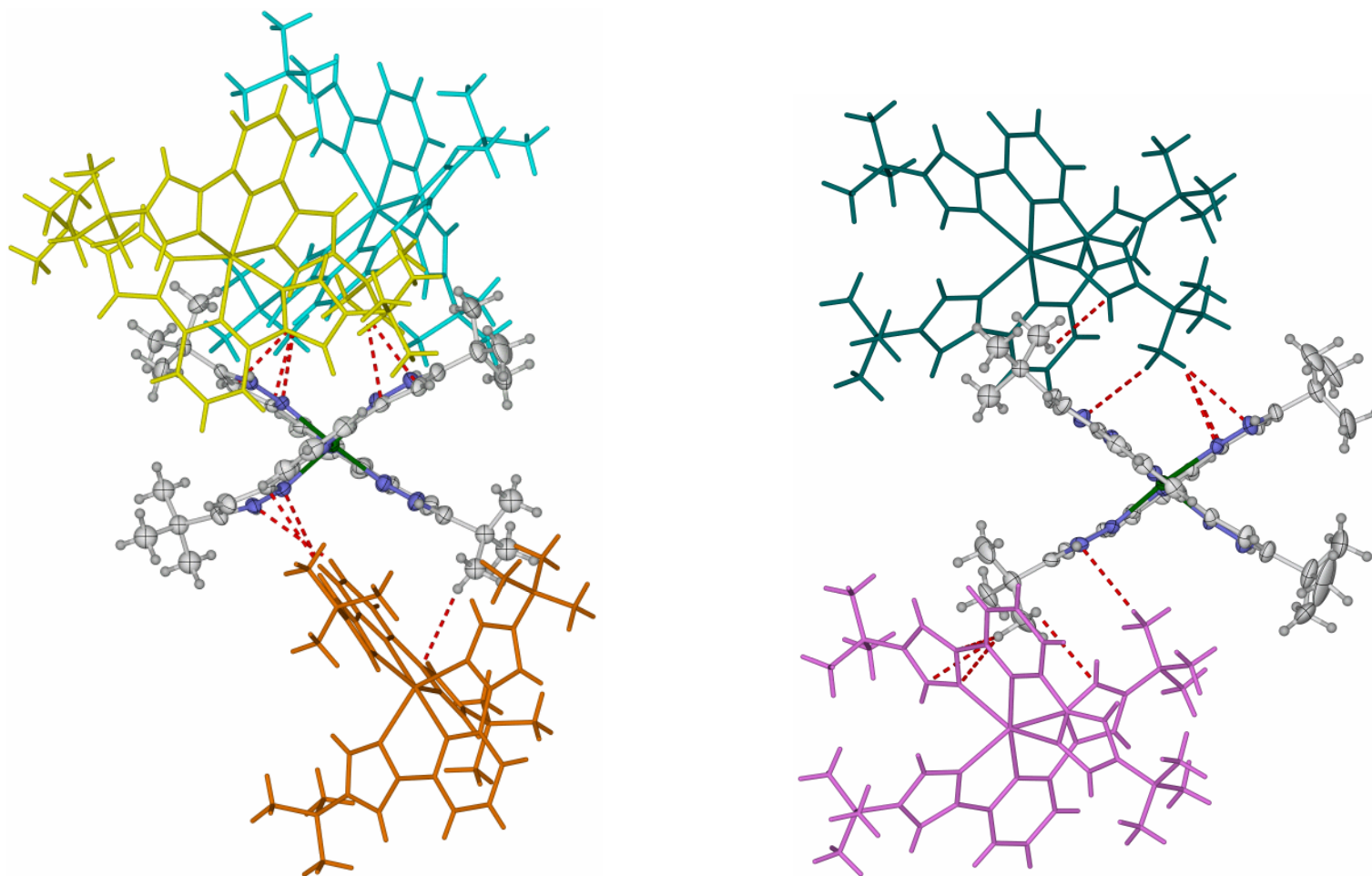


Fig. S5. View of complex molecules A (left) and B (right) in $\mathbf{3}[\text{BF}_4]_2 \cdot x\text{CF}_3\text{CH}_2\text{OH} \cdot y(\text{C}_3\text{H}_7)_2\text{O}$, emphasising the S-shaped L^3 ligand conformations and showing intermolecular contacts of 2.9–3.1 Å that may give rise to them. Only one orientation for disordered *tert*butyl groups is included.

Colour code: C, white; H, grey; Fe, green; N, blue. The neighbour molecules are molecule B (orange); molecule A, related by $1-x, \frac{1}{2}+y, \frac{1}{2}-z$ (yellow); molecule B, related by $\frac{1}{2}-x, 1-y, \frac{1}{2}+z$ (cyan); molecule B, related by $-\frac{1}{2}+x, \frac{1}{2}-y, -z$ (blue-green); and, molecule B, related by $\frac{1}{2}+x, \frac{1}{2}-y, -z$ (pink).

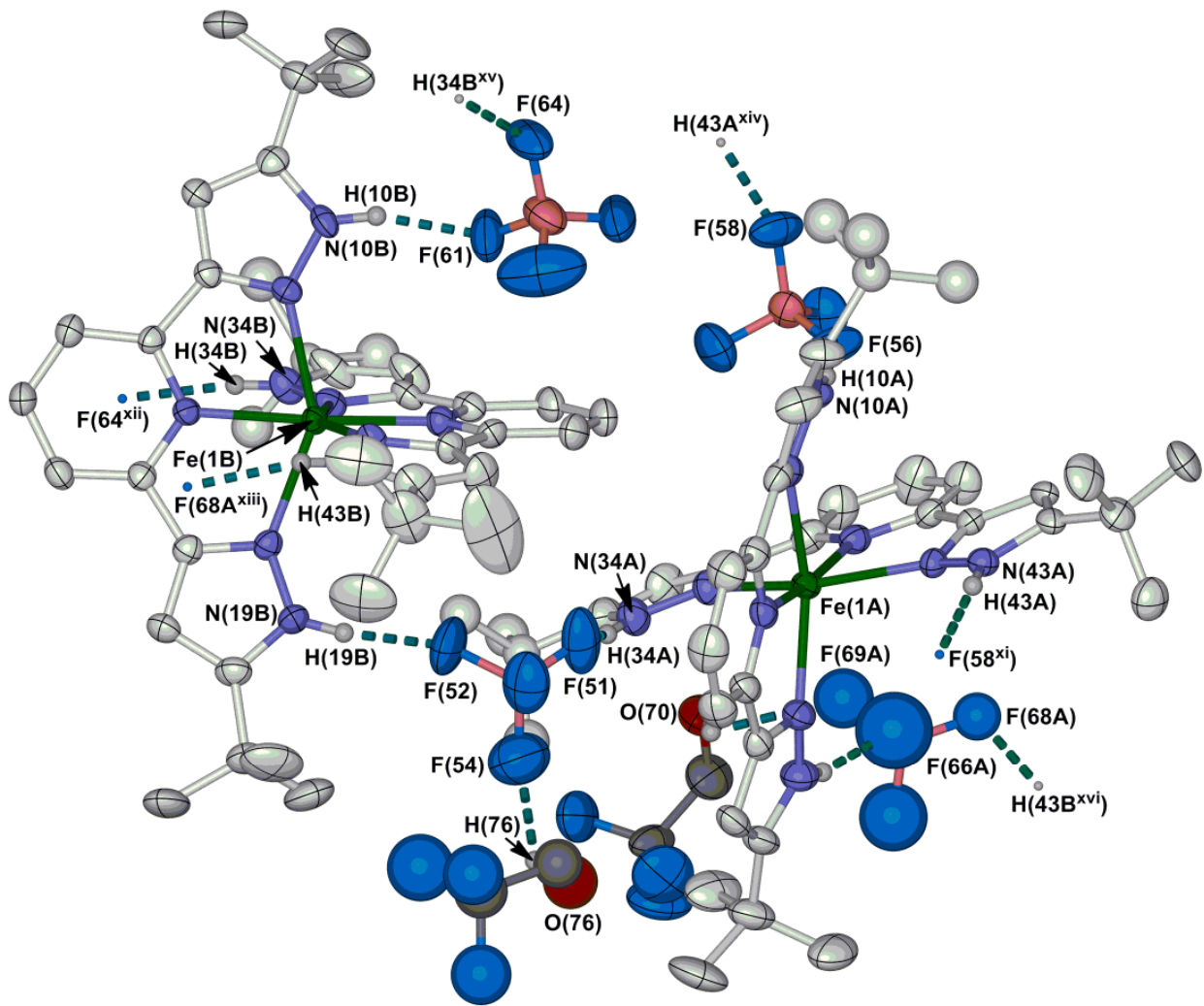


Fig. S6. View of the asymmetric unit of $3[\text{BF}_4]_2 \cdot x\text{CF}_3\text{CH}_2\text{OH} \cdot y(\text{C}_3\text{H}_7)_2\text{O}$. Atomic displacement ellipsoids are at the 50 % probability level. Only one orientation is included of the disordered *tert*butyl groups and anion, and the partial solvent sites that do not take part in hydrogen bonding interactions are not shown. C-bound H atoms have been omitted for clarity. Symmetry codes: (xi) $1-x, \frac{1}{2}+y, \frac{1}{2}-z$; (xii) $-\frac{1}{2}+x, \frac{1}{2}-y, -z$; (xiii) $\frac{1}{2}-x, 1-y, -\frac{1}{2}+z$; (xiv) $1-x, -\frac{1}{2}+y, \frac{1}{2}-z$; (xv) $\frac{1}{2}+x, \frac{1}{2}-y, -z$; (xvi) $\frac{1}{2}-x, 1-y, \frac{1}{2}+z$.

For clarity, only atoms involved in hydrogen bonding interactions are labelled in the Figure. Atoms N(43B) and H(70) are obscured in the view.

Colour code: C {complex}, white; C {solvent}, dark grey; H, pale grey; B, pink; F, cyan; Fe, green; N, pale blue; O, red.

The two 2,2,2-trifluoroethanol molecules shown are both only part-occupied.

Table S3 Selected bond lengths and angles in the crystal structure of **3**[BF₄]_xCF₃CH₂OH·y(C₃H₇)₂O (Å, °). See Figs. S4 for the atom numbering scheme.

	Molecule A	Molecule B
Fe(1)–N(2)	2.129(4)	2.170(3)
Fe(1)–N(9)	2.212(4)	2.243(3)
Fe(1)–N(18)	2.202(4)	2.271(3)
Fe(1)–N(26)	2.146(4)	2.166(3)
Fe(1)–N(33)	2.183(4)	2.267(4)
Fe(1)–N(42)	2.224(3)	2.202(3)
N(2)–Fe(1)–N(9)	73.91(14)	74.02(12)
N(2)–Fe(1)–N(18)	74.39(15)	73.16(13)
N(2)–Fe(1)–N(26) (ϕ)	170.27(13)	171.85(13)
N(2)–Fe(1)–N(33)	110.24(14)	99.04(13)
N(2)–Fe(1)–N(42)	101.20(13)	113.88(13)
N(9)–Fe(1)–N(18)	148.29(15)	146.93(13)
N(9)–Fe(1)–N(26)	97.11(14)	102.36(13)
N(9)–Fe(1)–N(33)	102.32(13)	83.97(13)
N(9)–Fe(1)–N(42)	84.29(13)	104.55(13)
N(18)–Fe(1)–N(26)	114.55(14)	110.71(13)
N(18)–Fe(1)–N(33)	88.13(14)	105.05(12)
N(18)–Fe(1)–N(42)	102.38(13)	85.22(13)
N(26)–Fe(1)–N(33)	74.91(14)	73.15(13)
N(26)–Fe(1)–N(42)	73.72(13)	73.96(13)
N(33)–Fe(1)–N(42)	148.51(14)	147.08(13)
θ	68.02(5)	71.47(4)

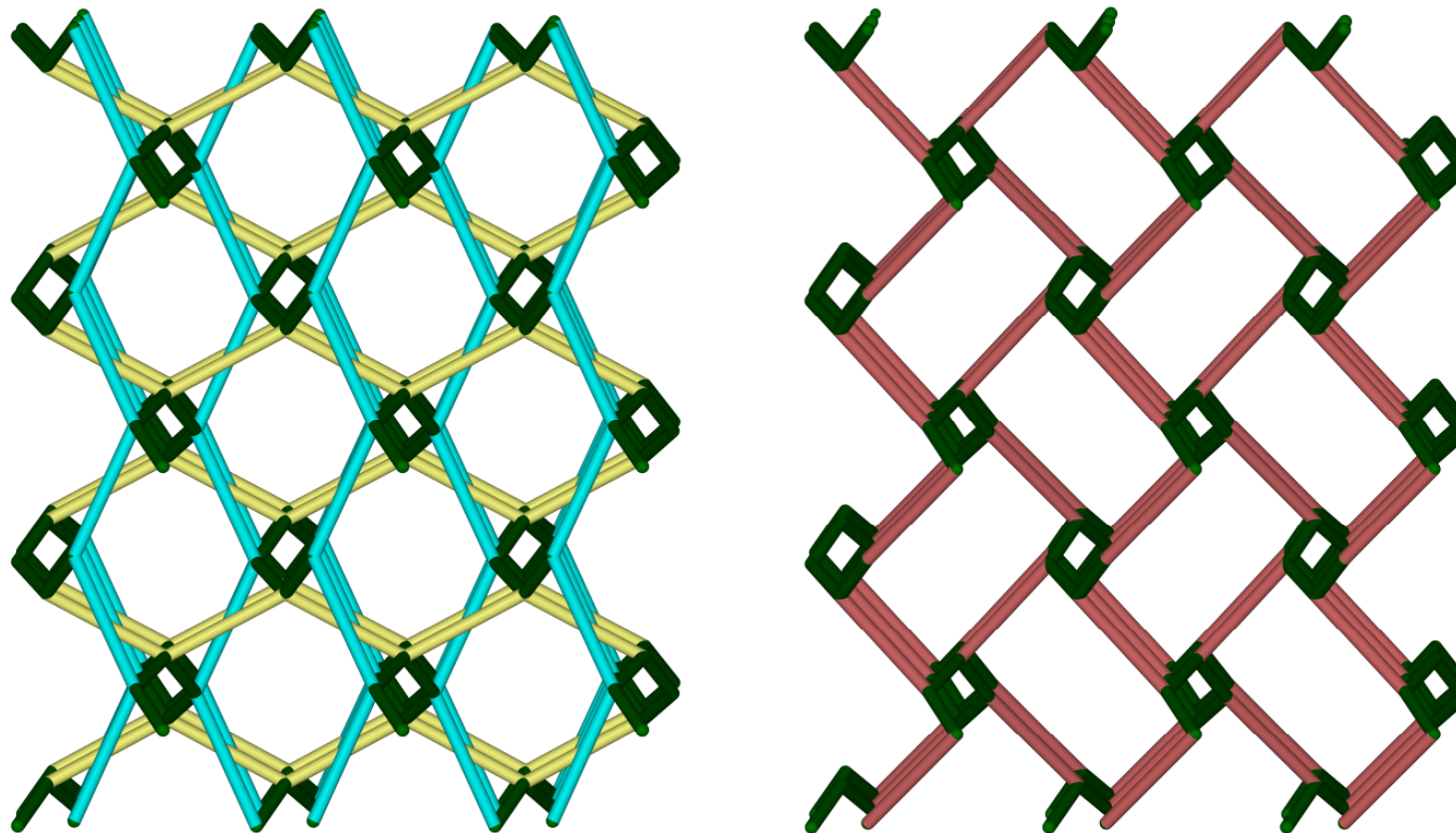


Fig. S7. Left: view of the helical, interpenetrating hydrogen bonded topology in $\mathbf{3}[\text{BF}_4]_2 \cdot x\text{CF}_3\text{CH}_2\text{OH} \cdot y(\text{C}_3\text{H}_7)_2\text{O}$. The A...B connections forming the helices are green, the while A...A (cyan) and B...B (yellow) connections link the helices in a self-penetrating manner. Right: View of a (10,3)-a net generated from the same coordinates, but with the A...A and B...B connections between helices in $\mathbf{3}[\text{BF}_4]_2 \cdot x\text{CF}_3\text{CH}_2\text{OH} \cdot y(\text{C}_3\text{H}_7)_2\text{O}$ replaced by an inter-helix A...B connection (pink).

The left hand view is the same as Fig. 5 in the main paper. The topology in $\mathbf{3}[\text{BF}_4]_2 \cdot x\text{CF}_3\text{CH}_2\text{OH} \cdot y(\text{C}_3\text{H}_7)_2\text{O}$ is related to the (10,3)-a net, but with the unique inter-helix A...B connection replaced by inter-helix A...A and B...B linkages.

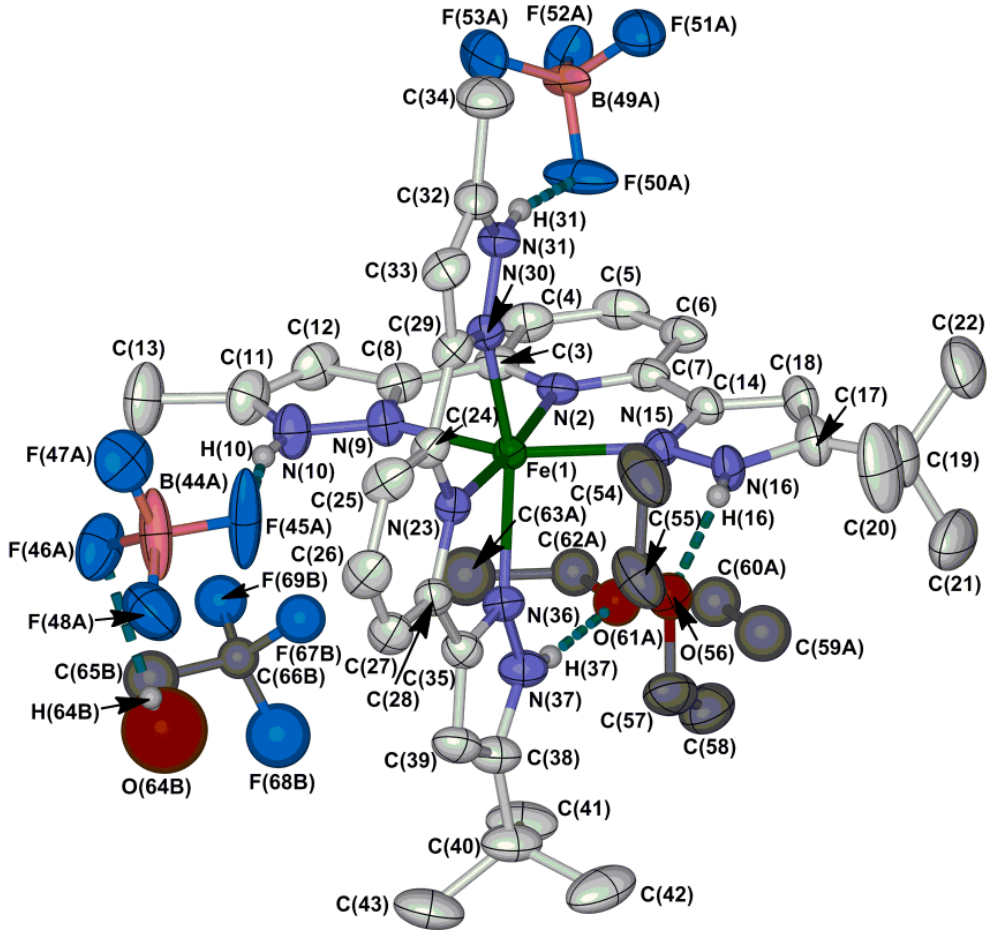


Fig. S8. View of the $[\text{Fe}(\text{L}^4)_2][\text{BF}_4]_2 \cdot 2(\text{C}_2\text{H}_5)_2\text{O} \cdot \text{CF}_3\text{CH}_2\text{OH}$ assembly in $[\text{Fe}(\text{L}^4)_2][\text{BF}_4]_2 \cdot x\text{CF}_3\text{CH}_2\text{OH} \cdot y(\text{C}_2\text{H}_5)_2\text{O}$, showing the full atom numbering scheme. Atomic displacement ellipsoids are at the 50 % probability level. Only one orientation of the disordered anions and solvent sites is included, and C-bound H atoms have been omitted for clarity.

Colour code: C {complex}, white; C {solvent}, dark grey; H, pale grey; B, pink; F, cyan; Fe, green; N {complex}, pale blue; N {solvent}, dark blue; O, red.

The 2,2,2-trifluoroethanol molecule shown [O(64B)-F(69B)] is only 0.25-occupied. A partial diethyl ether molecule also occupies that lattice site in the model, but is not included in the Figure.

Table S4 Selected bond lengths and angles in the crystal structure of **4**[BF₄]₂·xCF₃CH₂OH·y(C₂H₅)₂O (Å, °). See Fig. S8 for the atom numbering scheme.

Fe(1)–N(2)	2.116(3)
Fe(1)–N(9)	2.187(3)
Fe(1)–N(15)	2.188(3)
Fe(1)–N(23)	2.119(3)
Fe(1)–N(30)	2.184(3)
Fe(1)–N(36)	2.187(3)
N(2)–Fe(1)–N(9)	74.27(11)
N(2)–Fe(1)–N(15)	75.14(11)
N(2)–Fe(1)–N(23) (ϕ)	174.33(10)
N(2)–Fe(1)–N(30)	101.51(10)
N(2)–Fe(1)–N(36)	109.81(10)
N(9)–Fe(1)–N(15)	149.41(11)
N(9)–Fe(1)–N(23)	102.14(10)
N(9)–Fe(1)–N(30)	91.71(11)
N(9)–Fe(1)–N(36)	95.28(11)
N(15)–Fe(1)–N(23)	108.35(10)
N(15)–Fe(1)–N(30)	94.26(10)
N(15)–Fe(1)–N(36)	95.05(11)
N(23)–Fe(1)–N(30)	73.99(10)
N(23)–Fe(1)–N(36)	74.66(11)
N(30)–Fe(1)–N(36)	148.65(11)
θ	88.85(3)

Table S5 Hydrogen bond parameters for the crystal structures in this work (Å, °).^a

	D–H	H...A	D...A	D–H...A
[Fe(L¹)₂][ClO₄]₂·2(C₂H₅)₂O·CH₃NO₂				
N(10)–H(10)...O(27)	0.857(16)	1.932(16)	2.7835(18)	172.6(18)
N(13)–H(13A)...O(23 ⁱⁱ)	0.827(16)	2.175(17)	2.991(2)	169(2)
N(13)–H(13B)...O(21 ⁱⁱⁱ)	0.827(17)	2.507(19)	3.217(2)	144.6(19)
N(16)–H(16)...O(22)	0.837(15)	2.116(16)	2.9153(19)	159.6(18)
N(19)–H(19A)...O(24)	0.852(17)	2.190(18)	3.001(2)	159(2)
N(19)–H(19B)...O(21 ^{iv})	0.839(17)	2.299(18)	3.125(2)	168(2)
N(19)–H(19B)...O(23 ^{iv})	0.839(17)	2.59(2)	3.222(2)	133(2)
[Fe(L²)₂][BF₄]₂·3CH₃CN				
N(10)–H(10)...F(70)	0.88	1.96	2.8095(16)	160.5
N(13)–H(13)...F(71)	0.88	2.10	2.9025(16)	151.2
N(22)–H(22)...O(27)	0.88	2.15	2.6851(15)	118.5
N(22)–H(22)...N(80)	0.88	2.13	2.925(2)	150.7
N(25)–H(25)...F(63)	0.88	2.08	2.9047(17)	155.4
N(40)–H(40)...O(45)	0.88	2.17	2.6906(16)	117.5
N(40)–H(40)...N(74)	0.88	2.24	2.995(2)	143.5
N(43)–H(43)...F(69 ^{viii})	0.88	2.11	2.9281(18)	154.5
N(52)–H(52)...O(57)	0.88	2.05	2.6014(15)	119.8
N(55)–H(55)...F(65 ^{ix})	0.88	2.12	2.9192(16)	150.8
[Fe(L²)₂][ClO₄]₂·3CH₃CN				
N(10)–H(10)...O(70)	0.88	2.04	2.882(3)	160.3
N(13)–H(13)...O(71)	0.88	2.19	2.998(3)	152.5
N(22)–H(22)...O(27)	0.88	2.16	2.696(2)	118.5
N(22)–H(22)...N(80)	0.88	2.14	2.938(4)	151.1
N(25)–H(25)...O(63)	0.88	2.14	2.958(4)	154.1
N(40)–H(40)...O(45)	0.88	2.19	2.712(3)	118.0
N(40)–H(40)...N(74)	0.88	2.24	3.002(4)	144.0
N(43)–H(43)...O(69 ^{viii})	0.88	2.19	3.013(3)	154.9
N(52)–H(52)...O(57)	0.88	2.07	2.616(3)	119.6
N(55)–H(55)...O(65 ^{ix})	0.88	2.22	3.037(3)	153.8
[Fe(L³)₂][BF₄]₂·xCF₃CH₂OH·y(C₃H₇)₂O				
N(10A)–H(10A)...F(56)	0.88	2.02	2.886(5)	169.5
N(19A)–H(19A)...F(66A)/F(66B)	0.88	1.91/2.02	2.730(14)/2.810(9)	155.0/149.7
N(34A)–H(34A)...F(51)	0.88	2.03	2.847(6)	154.1
N(43A)–H(43A)...F(58 ^{xii})	0.88	1.92	2.787(5)	167.3
N(10B)–H(10B)...F(61)	0.88	1.96	2.799(5)	158.8
N(19B)–H(19B)...F(52)	0.88	1.95	2.768(5)	154.9
N(34B)–H(34B)...F(64 ^{xii})	0.88	1.97	2.828(5)	165.1
N(43B)–H(43B)...F(68A ^{xiii})/F(68B ^{xiii})	0.88	1.98/2.25	2.830(8)/3.101(15)	162.9/163.5
N(43B)–H(43B)...F(67B ^{xiii})	0.88	2.57	3.281(14)	138.8
O(70)–H(70)...F(69B)	0.84	2.27	2.749(15)	116.4
O(76)–H(76)...F(54)	0.84	2.14	2.824(12)	138.8
[Fe(L⁴)₂][BF₄]₂·xCF₃CH₂OH·y(C₂H₅)₂O				
N(10)–H(10)...F(45A)/F(45B)	0.88	1.90/2.16	2.740(6) 2.990(16)	160.0/155.9
N(16)–H(16)...O(56)	0.88	2.04	2.868(4)	157.0
N(31)–H(31)...F(50A)/F(50B)	0.88	1.95/1.95	2.801(7)/2.800(13)	163.9/163.0
N(37)–H(37)...O(61A)/O(61B)	0.88	1.94/2.09	2.797(7)/2.923(7)	165.9/158.2
O(64B)–H(64D)...F(46A)/F(48B)	0.84	2.35/1.80	3.04(3)/2.55(4)	140.5/146.3

^aSymmetry codes: (ii) $1/2+x, 3/2-y, -z$; (iii) $1/2+x, 1/2+y, 1/2-z$; (iv) $x, 1-y, 1/2+z$; (viii) $-x, -y, -z$; (ix) $-1+x, y, z$; (xi) $1-x, 1/2+y, 1/2-z$; (xii) $-1/2+x, 1/2-y, -z$; (xiii) $1/2-x, 1-y, -1/2+z$.

Table S6 Connections making up the hydrogen-bonded networks in this study (\AA). The symmetry codes are consistent with the other Figures and Tables in the ESI and the main paper.

	Distance between nodes (\AA)
1 [ClO ₄] ₂ ·2(C ₂ H ₅) ₂ O·CH ₃ NO ₂ (connections between complex dications and ClO ₄ ⁻ anions)	
N(13)–H(13A)...O(23 ⁱⁱ) = N(13 ⁱ)–H(13A ⁱ)...O(23 ^{xvii}) = O(23)...H(13A ^v)–N(13 ^v)	Fe(1)...Cl(20 ⁱⁱ) = Fe(1)...Cl(20 ^{xvii}) = Cl(20)...Fe(1 ^v) = 8.0009(5)
N(13)–H(13B)...O(21 ⁱⁱⁱ) = N(13 ⁱ)–H(13B ⁱ)...O(21 ^{xviii}) = O(21)...H(13B ^{vii})–N(13 ^{vii})	Fe(1)...Cl(20 ⁱⁱⁱ) = Fe(1)...Cl(20 ^{xviii}) = Cl(20)...Fe(1 ^{vii}) = 8.1777(6)
N(16)–H(16)...O(22)/N(19)–H(19A)...O(24) = N(16 ⁱ)–H(16 ⁱ)...O(22 ⁱ)/N(19 ⁱ)–H(19A ⁱ)...O(24 ⁱ)	Fe(1)...Cl(20) = Fe(1)...Cl(20 ⁱ) = 5.8786(5)
N(19)–H(19B)...O(21 ^{iv})/N(19)–H(19B)...O(23 ^{iv}) = N(19 ⁱ)–H(19B ⁱ)...O(21 ^{xix})/N(19 ⁱ)–H(19B ⁱ)...O(23 ^{xix}) = O(21)/O(23)...H(19B ^{vi})–N(19 ^{vi})	Fe(1)...Cl(20 ^{iv}) = Fe(1)...Cl(20 ^{xix}) = Cl(20)...Fe(1 ^{vi}) = 9.1901(5)
2 [BF ₄] ₂ ·3CH ₃ CN (connections between complex dications <i>via</i> bridging BF ₄ ⁻ ions)	
N(10)–H(10)...F(70)/N(13)–H(13)...F(71) and F(69)...H(43 ^{viii})–N(43 ^{viii}) = N(43)–H(43)...F(69 ^{viii}) and F(70 ^{viii})...H(10 ^{viii})–N(10 ^{viii})/F(71 ^{viii})...H(13 ^{viii})–N(13 ^{viii}) ^b	Fe(1)...Fe(1 ^{viii}) = 10.4927(5) ^b
N(25)–H(25)...F(63) and F(65)...H(55 ^x)–N(55 ^x) = N(55)–H(55)...F(65 ^{ix}) and F(63 ^{ix})...H(25 ^{ix})–N(25 ^{ix})	Fe(1)...Fe(1 ^x) = Fe(1)...Fe(1 ^{ix}) = 12.8890(4)
2 [ClO ₄] ₂ ·3CH ₃ CN (connections between complex dications <i>via</i> bridging ClO ₄ ⁻ ions)	
N(10)–H(10)...O(70)/N(13)–H(13)...O(71) and O(69)...H(43 ^{viii})–N(43 ^{viii}) = N(43)–H(43)...O(69 ^{viii}) and O(70 ^{viii})...H(10 ^{viii})–N(10 ^{viii})/O(71 ^{viii})...H(13 ^{viii})–N(13 ^{viii}) ^b	Fe(1)...Fe(1 ^{viii}) = 10.599(2) ^b
N(25)–H(25)...O(63) and O(65)...H(55 ^x)–N(55 ^x) = N(55)–H(55)...O(65 ^{ix}) and O(63 ^{ix})...H(25 ^{ix})–N(25 ^{ix})	Fe(1)...Fe(1 ^x) = Fe(1)...Fe(1 ^{ix}) = 12.995(2)
3 [BF ₄] ₂ ·xCF ₃ CH ₂ OH·y(C ₃ H ₇) ₂ O (connections between complex dications <i>via</i> bridging BF ₄ ⁻ ions)	
N(10A)–H(10A)...F(56) and F(58)...H(43A ^{xiv})–N(43A ^{xiv}) = N(43A)–H(43A)...F(58 ^{xi}) and F(56 ^{xi})...H(10A ^{xi})–N(10A ^{xi})	Fe(1A)...Fe(1A ^{xvi}) = Fe(1A)...Fe(1A ^{xi}) = 10.731(1)
N(19A)–H(19A)...F(66A)/F(66B) and F(68A)/F(68B)...H(43B ^{xvi})–N(43B ^{xvi}) = N(43B)–H(43B)...F(68A ^{xiii})/F(68B ^{xiii}) and F(66A ^{xiii})/F(66B ^{xiii})...H(19A ^{xiii})–N(19A ^{xiii})	Fe(1A)...Fe(1B ^{xvi}) = Fe(1B)...Fe(1A ^{xiii}) = 8.761(1)
N(34A)–H(34A)...F(51) and F(52)...H(19B)–N(19B)	Fe(1A)...Fe(1B) = 8.768(1)
N(10B)–H(10B)...F(61) and F(64)...N(34B ^{xv})–H(34B ^{xv}) = N(34B)–H(34B)...F(64 ^{xii}) and F(61 ^{xii})...N(10B ^{xii})–H(10B ^{xii})	Fe(1B)...Fe(1B ^{xv}) = Fe(1B)...Fe(1B ^{xii}) = 9.979(1)
^a Symmetry codes: (i) 1–x, y, 1/2–z; (ii) 1/2+x, 3/2–y, –z; (iii) 1/2+x, 1/2+y, 1/2–z; (iv) x, 1–y, 1/2+z; (v) –1/2+x, 3/2–y, –z; (vi) x, 1–y, –1/2+z; (vii) –1/2+x, –1/2+y, 1/2–z; (viii) –x, –y, –z; (ix) –1+x, y, z; (x) 1+x, y, z; (xi) 1–x, 1/2+y, 1/2–z; (xii) –1/2+x, 1/2–y, –z; (xiii) 1/2–x, 1–y, –1/2+z; (xiv) 1–x, –1/2+y, 1/2–z; (xv) 1/2+x, 1/2–y, –z; (xvi) 1/2–x, 1–y, 1/2+z; (xvii) 1/2–x, 3/2–y, 1/2+z; (xviii) 1/2–x, 1/2+y, z; (xix) 1–x, 1–y, –z. ^b Centrosymmetric pair.	

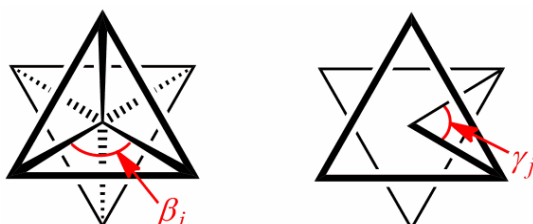
Definitions of the structural parameters discussed in the main paper.

α is the average of the four internal *cis*-N–Fe–N angles within the two chelate ligands, which increases from *ca.* 73° in the high-spin state to 80° in the low-spin state. Σ and Θ are defined as follows:

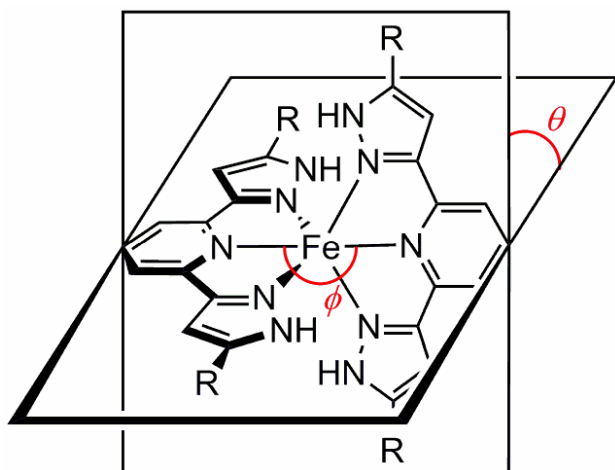
$$\Sigma = \sum_{i=1}^{12} |90 - \beta_i| \quad \Theta = \sum_{j=1}^{24} |60 - \gamma_j|$$

where β_i are the twelve *cis*-N–Fe–N angles about the iron atom and γ_j are the 24 unique N–Fe–N angles measured on the projection of two triangular faces of the octahedron along their common pseudo-threefold axis (Scheme S1). Σ is a general measure of the deviation of a metal ion from an ideal octahedral geometry, while Θ more specifically indicates its distortion towards a trigonal prismatic structure. A perfectly octahedral complex gives $\Sigma = \Theta = 0$.^[1,2]

Because the high-spin state of a complex has a much more plastic structure than the low-spin, this is reflected in Σ and Θ which are usually much larger in the high-spin state. The absolute values of these parameters depend on the metal/ligand combination in the compound under investigation, however.



Scheme S1. Angles used in the definitions of the coordination distortion parameters Σ and Θ .



Scheme S2. Definition of the Jahn-Teller distortion parameters θ and ϕ .^[2,3]

These two parameters define the magnitude of an angular Jahn-Teller distortion, that is often observed in high-spin $[\text{Fe}(1\text{-bpp})_2]^{2+}$ derivatives like **1** ($\theta \leq 90^\circ$, $\phi \leq 180^\circ$). Spin-crossover is inhibited if this angular distortion is too large, which usually means $\theta < 76$ and/or $\phi < 172^\circ$, because the associated rearrangement to a more regular low-spin coordination geometry cannot be accommodated by a rigid solid lattice.^[2]

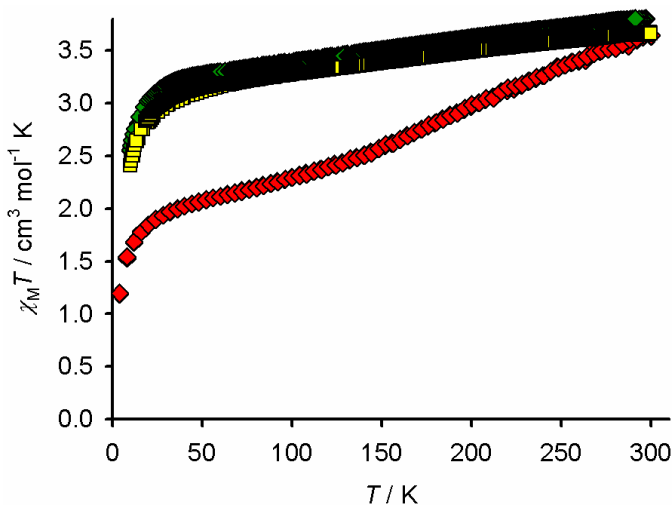


Fig. S9. Variable temperature magnetic susceptibility behaviour of **2**[BF₄]₂·H₂O (green diamonds), **2**[ClO₄]₂·2H₂O (yellow squares), **3**[BF₄]₂·H₂O (black circles) and **4**[BF₄]₂·½CF₃CH₂OH (red diamonds). See the main article for more details.

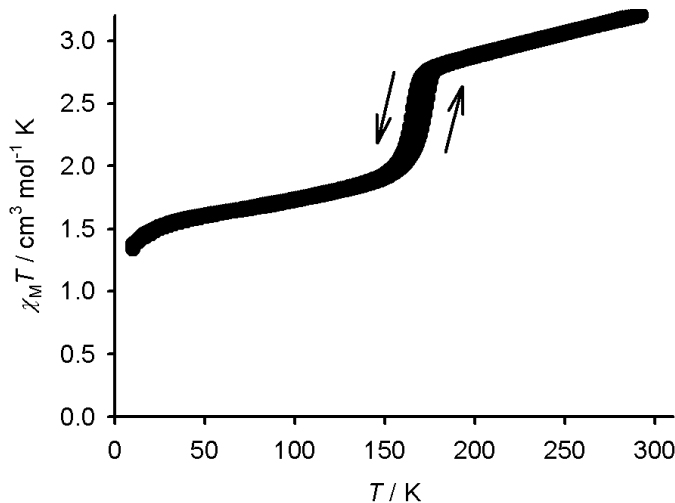


Fig. S10. Variable temperature magnetic susceptibility behaviour of **1**[ClO₄]₂·2H₂O. The sample was measured in both cooling and warming mode.

We interpret these data as showing a predominantly high-spin material, contaminated by *ca.* 30 % of a spin-crossover phase. Since the crystalline compound is high-spin at 150 K, most of the sample is probably material derived from that crystal form. The minor spin-crossover fraction may be a second phase of the iron(II) compound, or an aerobic decomposition product. Since the freshly prepared samples only contain one crystal morphology, and the complex is air-sensitive, we prefer the latter explanation.

References

- [1] a) J. K. McCusker, A. L. Rheingold and D. N. Hendrickson, *Inorg. Chem.*, 1996, **35**, 2100;
 b) P. Guionneau, M. Marchivie, G. Bravic, J.-F. Létard and D. Chasseau, *Top. Curr. Chem.*, 2004, **234**, 97.
- [2] M. A. Halcrow, *Coord. Chem. Rev.*, 2009, **253**, 2493.
- [3] a) J. M. Holland, J. A. McAllister, C. A. Kilner, M. Thornton-Pett, A. J. Bridgeman and M. A. Halcrow, *J. Chem. Soc. Dalton Trans.*, 2002, 548;
 b) J. Elhaïk D. J. Evans, C. A. Kilner and M. A. Halcrow, *Dalton Trans.*, 2005, 1693;
 c) C. A. Kilner and M. A. Halcrow, *Polyhedron*, 2006, **25**, 235;
 d) M. Haryono, F. W. Heinemann, K. Petukhov, K. Gieb, P. Müller and A. Grohmann, *Eur. J. Inorg. Chem.*, 2009, 2136.